molecules

MDPI

Article

Antitumor Effects of *Juncus effusus* L. subsp. *effusus* in a Mammary Tumor Model: Regulation of ERα, p53, PCNA, and HIF-1α

İrem Ergin [1,*], Mürşide Ayşe Demirel [2], İpek Süntar [3,*], Saadet Özen Akarca Dizakar [4], Osman Tugay [5], Kevser Taban [6] and Oytun Okan Şenel [1]

1 Department of Surgery, Faculty of Veterinary Medicine, Ankara University, Ankara 06070, Türkiye; osenel@veterinary.ankara.edu.tr
2 Department of Basic Pharmaceutical Sciences, Faculty of Pharmacy, Gazi University, Ankara 06330, Türkiye; aysedemirel@gazi.edu.tr
3 Department of Pharmacognosy, Faculty of Pharmacy, Gazi University, Ankara 06330, Türkiye
4 Department of Histology and Embryology, Faculty of Medicine, Bakırçay University, Izmir 35665, Türkiye; ozen.akarca@bakircay.edu.tr
5 Department of Pharmaceutical Botany, Faculty of Pharmacy, Selçuk University, Konya 42130, Türkiye; otugay@selcuk.edu.tr
6 Department of Pharmacognosy, Faculty of Pharmacy, Sivas Cumhuriyet University, Sivas 58140, Türkiye; kevsertabann@gmail.com
* Correspondence: ergin@ankara.edu.tr (İ.E.); ipesin@gazi.edu.tr (İ.S.)

Abstract

Estrogen receptor-positive breast cancer remains difficult to treat, driving the search for new therapeutic agents. *Juncus effusus* L., a medicinal plant rich in bioactive constituents, has shown preliminary anticancer activity, yet its efficacy in hormone-responsive tumor models in vivo has not been established. We evaluated the antitumor effects of the ethyl acetate sub-extract of *J. effusus* L. subsp. *effusus* in an N-methyl-N-nitrosourea (NMU)-induced rat mammary tumor model, assessing tumor burden, histopathology, and molecular markers. Thirty-six Sprague–Dawley rats were divided into six groups (n = 6): sham, control, reference, and three groups receiving the sub-extract at 100, 200, or 400 mg/kg. After NMU induction (50 mg/kg), treatment began once tumor volumes reached approximately 2000 mm^3 and continued for eight weeks. The 200 mg/kg dose markedly reduced tumor volume relative to control ($p < 0.0001$) and lowered both ERα and PCNA expression ($p < 0.001$ and $p < 0.0001$). The 100 and 200 mg/kg groups also showed lower p53 and ERα mRNA levels than the other treatment groups. HIF-1α, though elevated in control tumors, declined only modestly and without statistical significance after treatment. These results indicate that *J. effusus* subsp. *effusus*, particularly at 200 mg/kg, suppresses proliferation and modulates ERα- and p53 expression, supporting its potential for further preclinical investigation.

Keywords: estrogens; flavonoids; mammary tumor; medical plants; oncoproteins

Check for updates

Academic Editors: Kuniyoshi Shimizu and Yhiya Amen

Received: 23 June 2026
Revised: 13 July 2026
Accepted: 20 July 2026
Published: 24 July 2026

Copyright: © 2026 by the authors. Licensee MDPI, Basel, Switzerland. This article is an open access article distributed under the terms and conditions of the Creative Commons Attribution (CC BY) license.

1. Introduction

Breast cancer remains the most commonly diagnosed malignancy among women worldwide, with estrogen receptor (ER)-positive tumors constituting the majority of newly reported cases in recent years [1,2]. Current therapeutic approaches for ER-positive breast cancer mainly rely on endocrine-modulating agents, such as selective estrogen receptor

modulators (e.g., tamoxifen) and aromatase inhibitors [3,4]. Despite their clinical efficacy, these treatments are often associated with adverse effects, reduced tolerability, and substantial economic burden, which may compromise long-term adherence and therapeutic outcomes [5]. In this context, increasing attention has been directed toward natural compounds with estrogen-modulating potential, particularly phytoestrogens, due to their structural similarity to endogenous estrogens, relatively favorable safety profiles, and pleiotropic biological activities [6].

Among plant-derived resources investigated for their pharmacological potential, members of the genus *Juncus* have attracted increasing scientific interest due to their rich phytochemical profile, including phytoestrogens and other bioactive compounds, and their broad spectrum of biological activities [7,8]. The genus *Juncus* (Juncaceae) is an expansive taxon comprising numerous biologically active species, such as *J. gerardii* [8], *J. inflexus* [9], and *J. maritimus* [10]. In addition, *Juncus effusus* L. has attracted particular attention due to its extensive history in various traditional medicine systems, where it has been utilized for its anti-inflammatory, antipyretic, and diuretic effects [11]. It grows naturally in certain regions of Türkiye, where it is locally referred to as "Has Kofa" [12,13]. Phytochemical studies have revealed that *J. effusus* L. contains a rich composition of bioactive metabolites, including flavones, phenolic acids, p-hydroxybenzaldehyde, cycloartane triterpenoids, dihydrodibenzoxepins, and phenanthrene derivatives [7,11]. These compounds have been associated with notable antioxidant, anti-inflammatory, and antiproliferative activities, positioning *J. effusus* L. as a promising candidate for further investigation of plant-derived bioactivities with potential relevance to oncology.

Breast cancer development and progression involve multiple biological processes, including dysregulated cell proliferation, impaired apoptosis, hormone-dependent signaling, and adaptation to the tumor microenvironment. Evaluating the antitumor efficacy of candidate agents therefore requires biomarkers that reflect these key aspects of tumor biology. Estrogen receptor alpha (ERα), p53, proliferating cell nuclear antigen (PCNA), and hypoxia-inducible factor-1 alpha (HIF-1α) are well-established biomarkers associated with different molecular pathways involved in breast cancer progression. ERα is the principal mediator of estrogen-dependent tumor growth in ER-positive breast cancer and the primary target of endocrine therapy, making it particularly relevant for investigating the effects of phytoestrogen-containing compounds [14,15]. As a key tumor suppressor, p53 regulates cell-cycle arrest, apoptosis, and DNA repair, thereby providing insight into tumor cell responses to therapeutic intervention [16]. PCNA is widely recognized as a marker of cellular proliferation because of its essential role in DNA replication and cell-cycle progression [17]. In contrast, HIF-1α is a central regulator of the hypoxic response that promotes angiogenesis, metabolic reprogramming, and tumor progression, reflecting adaptive changes within the tumor microenvironment [18]. Because these biomarkers reflect different biological processes involved in breast cancer progression, evaluating them together allows a more comprehensive assessment of the antitumor effects of candidate agents.

Although several in vitro studies have reported that *J. effusus* extracts exert cytotoxic and antiproliferative effects in mammary tumor cell lines, there is a lack of in vivo evidence supporting their antitumor efficacy in biologically relevant breast cancer models. Based on its reported antioxidant, anti-inflammatory, and antiproliferative properties, we hypothesized that *J. effusus* L. subsp. *effusus* would suppress mammary tumor progression by reducing cellular proliferation and promoting apoptotic responses in vivo. Therefore, this study aimed to evaluate the antitumor potential of *J. effusus* subsp. *effusus* in an N-methyl-N-nitrosourea (NMU)-induced mammary tumor model in rats. To elucidate the underlying mechanisms, we assessed its effects on proliferative and apoptotic pathways,

alongside histopathological alterations, immunohistochemical markers (ERα, p53, PCNA, and HIF-1α), and gene expression profiles (ERα and p53).

2. Materials and Methods

2.1. Chemicals

N-nitroso-N-methylurea (NMU) (CAS No.: 684-93-5, Cat. No.: HY-34758) and tamoxifen citrate (CAS No.: 10540-29-1, Cat. No.: HY-13757A) were purchased from MedChemExpress (Monmouth Junction, NJ, USA). Xylazine hydrochloride (Xylazine Bio® 2%, Bioveta, Ivanovice na Hané, Czech Republic) and ketamine hydrochloride (Ketasol® 10%, Richter Pharma AG, Wels, Austria) were used for anesthesia. Primary antibodies against ER-α (Cat. No.: E-AB-15624-120), p53 (Cat. No.: E-AB-65674-120), PCNA (Cat. No.: E-AB-64562-120), and HIF-1α (Cat. No.: E-AB-52265) were obtained from Elabscience Biotechnology Co., Ltd. (Wuhan, China).

2.2. Plant Material, Extraction, and Fractionation

Materials of *J. effusus* subsp. *effusus* were collected in September 2023 by Dr. Osman Tugay from the Bolu (near Lake Abant, 1350 m) and Artvin (between Şavşat and Ardahan) regions of Türkiye, and their scientific names were identified using the publications "Flora of Turkey and the East Aegean Islands" and "List of Turkish Plants" [19,20]. The specimens are stored at the Selçuk University Herbarium (KNYA 30.202 and KNYA 30.208).

The dried, powdered aerial parts (3589.57 g) were macerated at room temperature with 95% ethanol (1:14 *w*/*v*) in five consecutive 10 L batches for 48 h each, with intermittent agitation. The combined extracts were filtered and evaporated under reduced pressure at 40 °C to yield 606.28 g of crude extract (16.88% yield). The extract was suspended in water and partitioned with petroleum ether (discarded) and ethyl acetate. The crude extract was subsequently suspended in distilled water and successively partitioned with petroleum ether (discarded) and ethyl acetate. The ethyl acetate layer was collected, concentrated to dryness, and yielded 59.20 g of ethyl acetate extract (equivalent to 9.76% of the crude extract), which was used for the in vivo experiments.

2.3. Determination of Phenolic Compounds by UHPLC-ESI-MS/MS

Phenolic compounds in the extract were analyzed using ultra-high-performance liquid chromatography coupled with electrospray ionization tandem mass spectrometry (UHPLC-ESI-MS/MS), following the validated method of Can et al. [21]. Analyses were performed on an Agilent 1290 Infinity UHPLC system (G4226A autosampler, G1330B thermostat, G4204A quaternary pump with degasser, and G1316A temperature-controlled column compartment; Agilent Technologies, Santa Clara, CA, USA) coupled to an Agilent 6460 triple quadrupole mass spectrometer equipped with an electrospray ionization source. Data acquisition and processing were conducted using MassHunter Qualitative and Quantitative Analysis software (version B.07.00, Agilent Technologies, Santa Clara, CA, USA).

Chromatographic separation was achieved on a Zorbax SB-C18 analytical column (4.6 × 100 mm, 3.5 µm; Agilent Technologies, Santa Clara, CA, USA) at 30 °C. The mobile phase consisted of solvent A (water with 0.1% formic acid) and solvent B (acetonitrile with 0.1% formic acid). A gradient elution program was applied as follows: 5% B (0 min), 20% B (5 min), 90% B (10–13 min), returning to 5% B (14 min), and re-equilibrated at 5% B until 17 min. The flow rate was set to 0.4 mL/min. Calibration curves were constructed using seven concentration levels of standard compounds. The chromatographic and mass spectrometric conditions, as well as the method validation parameters (linearity, LOD, LOQ, precision, and recovery) were adopted directly from the fully validated method previously reported by Can et al. [21]. Since the extract was analyzed on the same instrument under

identical operational conditions, the validation data presented in that study are directly applicable to the quantification of compounds in our extract.

2.4. Animals

Thirty-six healthy 3-week-old female Sprague–Dawley rats (50–70 g) were obtained from the Experimental Animals Laboratory of Bilkent University. The animals were individually housed under controlled conditions (21–24 °C, 40–45% humidity, 12 h light/dark) at the Laboratory Animals Breeding and Experimental Research Center of the Faculty of Pharmacy, Gazi University, with free access to standard chow and water. Body weights were monitored weekly throughout the experimental period. Rats were acclimated for seven days before experimental induction. All procedures were conducted in accordance with institutional and international guidelines for the care and use of laboratory animals and were approved by Gazi University Animal Experiments Local Ethics Committee (Approval no: G.Ü.ET-22.054).

2.5. Experimental Design

A flowchart of the experimental procedure is given in Figure 1. After one week of acclimation, rats were randomly assigned to six groups: sham (S, n = 6), control (C, 0.5% carboxymethylcellulose [CMC], 1 mL/day, p.o., n = 6), reference (R, tamoxifen, 10 mg/kg/day, p.o., n = 6), *J. effusus* subsp. *effusus* 100 mg/kg/day sub-extract (J100, n = 6), *J. effusus* subsp. *effusus* 200 mg/kg/day sub-extract (J200, n = 6), and *J. effusus* subsp. *effusus* 400 mg/kg/day sub-extract (J400, n = 6). A single intraperitoneal dose of N-nitroso-N-methylurea was used to induce mammary tumors (NMU, 50 mg/kg in 1 mL saline) [22]. Mammary tumors were not induced in the S group.

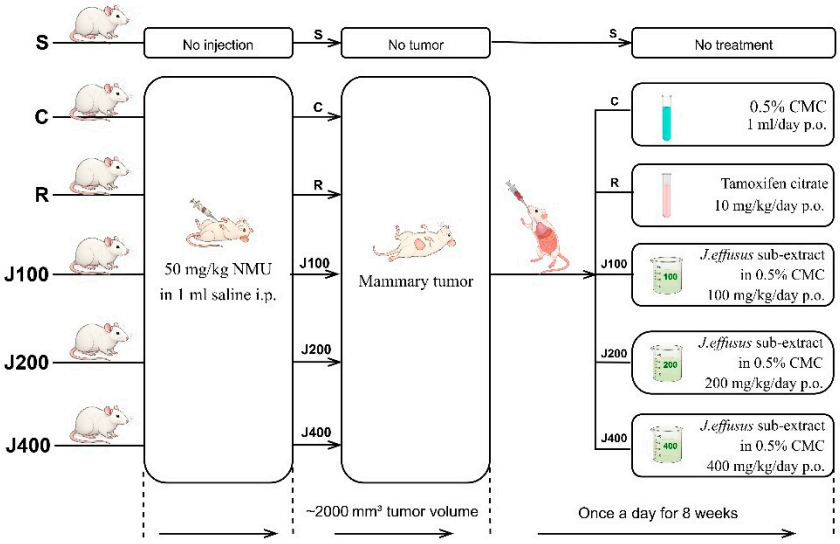


Figure 1. Flowchart of the experimental design, showing group allocation and study workflow.

Three weeks after NMU administration, the mammary glands of all animals were palpated weekly to monitor tumor development. Once tumor volume reached approximately ~2000 mm^3, treatment protocols were initiated and continued for 8 weeks [23]. Tumor size was measured weekly using a Vernier caliper. Tumor volume (V) was calculated according to the standard ellipsoid formula: $V\ (mm^3) = (L \times W^2)/2$, where L represents the longest diameter and W the shortest diameter of the tumor. When multiple tumors were present in a single animal, the volume of each tumor was calculated separately and summed to obtain the total tumor burden per animal, which was used for all subsequent analyses.

At the end of the experimental period, all rats were anesthetized with xylazine (10 mg/kg) and ketamine (80 mg/kg) and sacrificed by cardiac puncture-induced exsanguination. Mammary tissues were excised, fixed in 10% neutral-buffered formalin for histopathological assessment, and stored at −80 °C for subsequent gene expression analysis.

2.6. Histopathological Investigation

Formalin-fixed tissues were embedded in paraffin, and 4 µm-thick sections were prepared using a microtome (Slee CUT 5062, Slee Medical GmbH, Mainz, Germany). Sections were stained with hematoxylin and eosin for histopathological grading, and with Masson's Trichrome (Bio-Optica Milano S.p.A., Milan, Italy; Cat. No. BO 04-010802) to evaluate fibrosis [24,25]. Histological grading was assessed in 10 randomly selected high-power fields under a light microscope, according to the Nottingham Grading System (NGS), which evaluates mitotic activity, nuclear pleomorphism, and tubule formation (Table 1) [24].

Table 1. Nottingham Grading System [24].

Criteria	Score	Description
Mitosis counts	1	Fewer than 11 mitoses in 10 HPF
	2	Between 11 and 20 mitoses in 10 HPF
	3	Greater than 20 mitoses in 10 HPF
Nuclear pleomorphism	1	Small, regular, uniform cells
	2	Moderate increase in size and variability
	3	Marked variation
Tubule formation	1	More than 75% of the tumor
	2	10–75% of the tumor
	3	Less than 10% of the tumor

HPF: High-power field.

2.7. Immunohistochemical Analysis

Immunohistochemical staining was performed using the Anti-Polyvalent HRP (RTU) and DAB Substrate System kits (Lab Vision, Thermo Fisher Scientific, Fremont, CA, USA). Paraffin-embedded tissue sections were deparaffinized, rehydrated, and subjected to antigen retrieval in citrate buffer (pH 6.0; Thermo Fisher Scientific, Fremont, CA, USA; Cat. No. AP-9003-999) by heating at 95 °C for 20 min. After rinsing with distilled water, sections were incubated at 4 °C for 24 h in a humidified chamber with primary antibodies against ER-α, p53, PCNA, and HIF-1α (all 1:100). Following phosphate-buffered saline washes, sections were incubated with a secondary antibody solution (anti-mouse IgG/anti-rabbit IgG; Lab Vision, Thermo Scientific) for 10 min at room temperature. Immunoreactivity was visualized using 3,3′-diaminobenzidine tetrahydrochloride and counterstained with Mayer's hematoxylin. Slides were then mounted with Entellan (Merck, Darmstadt, Germany). Microscopic evaluation was performed using a ZEISS Axiolab 5 imaging system (Carl Zeiss Microscopy GmbH, Jena, Germany) with Zen Blue 3.4 software. Quantification of immunoreactivity in tumor tissue was carried out using the ImageJ software (version 1.54, National Institutes of Health, Bethesda, MD, USA), based on the method described by Santana-Krímskaya et al. [26].

2.8. p53 and ER-α Gene Expression in Mammary Tissue

Total RNA was extracted from mammary tissue samples using the DiaRex® Total RNA Extraction Kit (Cat. No: TR-0877, Diagen Biotechnology, Ankara, Türkiye), following the manufacturer's protocol. Approximately 5–30 mg of tissue was homogenized, and the resulting RNA (30–50 µL per sample) was stored at −80 °C until use. First-strand

complementary DNA (cDNA) synthesis was performed using the SOLIScript® RT cDNA Synthesis Kit (SOLIS BIODYNE, Tartu, Estonia) with 1 µg of total RNA input per 20 µL reaction. Each reaction included 2 µL of 10× RT buffer, 1 µL of reverse transcriptase, 0.5 µL of dNTP mix, 0.1 µL of RNase inhibitor, 1 µL of Oligo (dT) primers, and nuclease-free water to volume. Reverse transcription was carried out at 50 °C for 5 min, followed by enzyme inactivation at 85 °C for 5 min. Synthesized cDNA was stored at −20 °C for further use.

Quantitative real-time PCR (qRT-PCR) was conducted on a Bio-Rad CFX-96 Real-Time PCR Detection System (Bio-Rad Laboratories, Hercules, CA, USA) using the SensiFAST™ SYBR® No-ROX Kit (Bioline Reagents Ltd., London, UK). Each 20 µL PCR reaction contained 10 µL of 2× master mix, 5 µL of primer mix (0.5 µM), and 5 µL of diluted cDNA template. The thermal profile consisted of an initial denaturation at 95 °C for 5 min, followed by 40 cycles of denaturation at 95 °C for 5 s and annealing at 56 °C (for p53 and ERα) or 62 °C (for ACTB) for 30 s, with fluorescence acquisition at the end of each cycle. Relative gene expression levels were calculated using the $2^{-\Delta\Delta Ct}$ method. Statistical analyses and visualizations were performed using R software (v4.3.2) and the following packages: qpcrtools (v1.0.1), ggpubr (v0.6.0), dplyr (v1.1.4), tidyverse (v2.0.0), and car (v3.1-2) (Table 2).

Table 2. Primer sequences.

Gene	Forward Primer (5′ to 3′)	Reverse Primer (5′ to 3′)
p53	CGAGATGTTCCGAGAGCTGAATG	GTCTTCGGGTAGCTGGAGTG
ERα	TGCACCATCGATAAGAACC	GRCTCCTGAAGTGCCCATT
β-Actin	GAAGATCAAGATCATTGCTCCT	TGGAAGGTGGACAGTGAG

2.9. Statistical Analysis

Statistical analyses were performed using GraphPad Prism 8.0 (GraphPad Software, San Diego, CA, USA). Results were expressed as mean ± Standard Error of the Mean (SEM). The one-way ANOVA followed by Tukey's Multiple Comparison Test was used to determine the significance of differences among groups. Parametric assumptions were not met for the variables ER-α and p53 expressions; therefore, the statistical significance of differences among groups was assessed using the Kruskal–Wallis test, followed by Dunn–Bonferroni post hoc comparisons. Statistical significance was assumed at the level of $p < 0.05$.

3. Results

3.1. Phytochemical Analysis Results

A comprehensive phenolic composition of the ethyl acetate sub-fraction of *J. effusus* subsp. *effusus* was characterized using UHPLC-ESI-MS/MS analysis. The profiling confirmed the presence of multiple bioactive phenolic constituents, including quinic acid, chlorogenic acid, peonidin-3-*O*-glucoside, 4-Hydroxybenzoic acid, ferulic acid, *p*-coumaric acid, luteolin, and apigenin. The chromatographic separation of the sub-fraction is illustrated in Figure 2, and detailed analytical parameters for each identified compound, such as retention times, limits of detection and quantification (LOD/LOQ), and quantified concentrations in the extract (ng/mg), are summarized in Table 3 and Figure 3. Since quantification was based on the validated UHPLC-ESI-MS/MS protocol described by Can et al. [21], the MRM transitions, optimized instrument parameters, validation data, and representative chromatograms are summarized in the Supplementary Material (Table S1 and Figure S1).

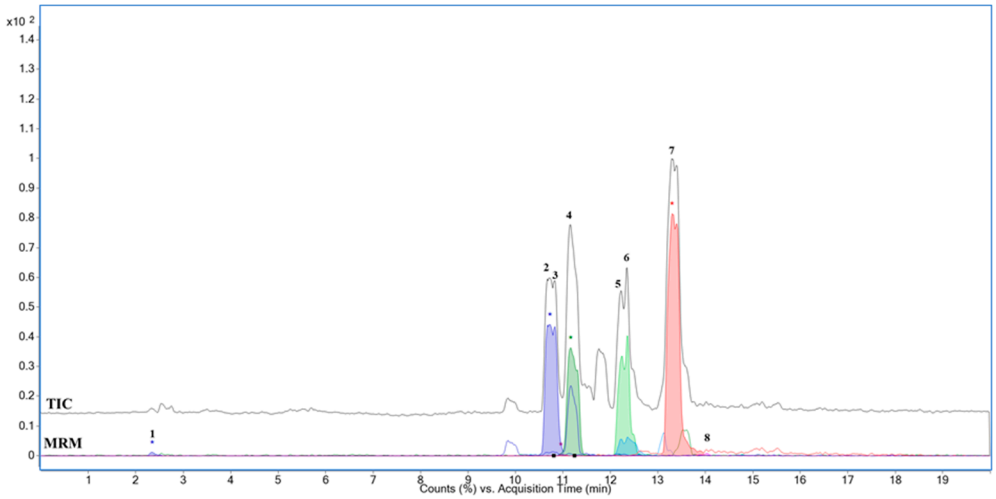


Figure 2. UHPLC-ESI-MS/MS TIC and MRM chromatograms of the ethyl acetate sub-extract of *J. effusus* subsp. *effusus* (1. Quinic acid, 2. Chlorogenic acid, 3. Peonidin-3-*O*-glucoside, 4. 4-Hydroxybenzoic acid, 5. Ferulic acid, 6. *p*-Coumaric acid, 7. Luteolin, 8. Apigenin).

Table 3. Determination of the phenolic constituents in the ethyl acetate sub-extract of *J. effusus* subsp. *effusus*.

Compounds	Retention Time	LOD/LOQ (μg/L)	Amounts of the Compounds in the Extract (ng/mg)
Quinic acid	2.344	0.84/2.80	2.40
Chlorogenic acid	10.729	0.41/1.37	41.52
Peonidin-3-*O*-glucoside	10.959	1.09/3.63	1.14
4-Hydroxybenzoic acid	11.160	1.24/4.13	52.35
Ferulic acid	12.360	1.30/4.35	31.23
p-Coumaric acid	12.362	0.90/3.00	14.90
Luteolin	13.298	0.54/1.81	12.71
Apigenin	14.038	1.09/3.65	0.05

LOD: Limit of Detection; LOQ: Limit of Quantification.

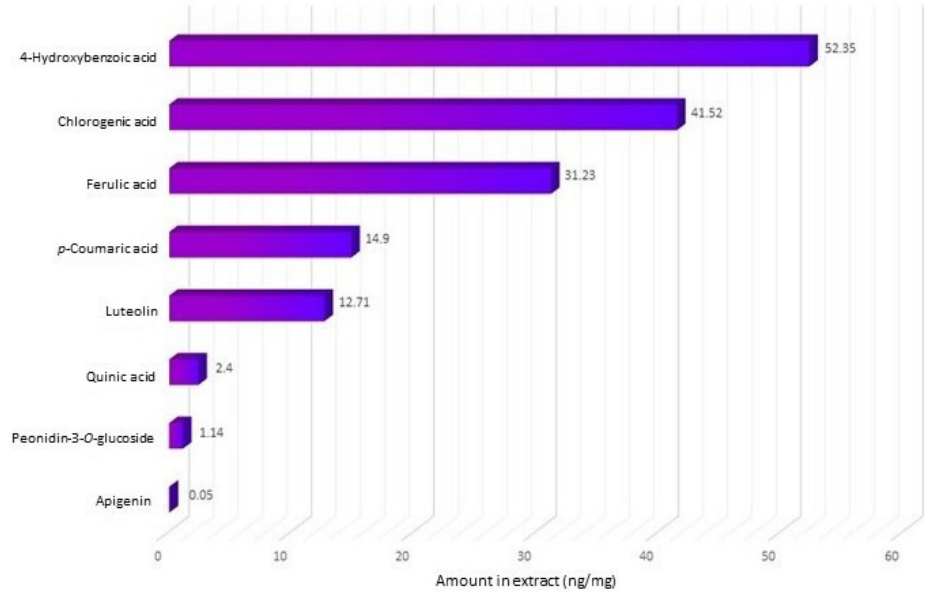


Figure 3. Amounts of the individual phenolic constituents (ng/mg) in the ethyl acetate sub-extract of *J. effusus* subsp. *effusus*, determined by UHPLC-ESI-MS/MS. Constituents are shown in descending order of abundance. The corresponding retention times and limits of detection/quantification (LOD/LOQ) are provided in Table 3.

3.2. Body Weight Measurements and Tumor Volume Analysis

Body weight increased gradually in all groups throughout the experimental period. Despite minor fluctuations, no marked differences in body weight were observed among the S, C, R, J100, J200, and J400 groups (Figure 4).

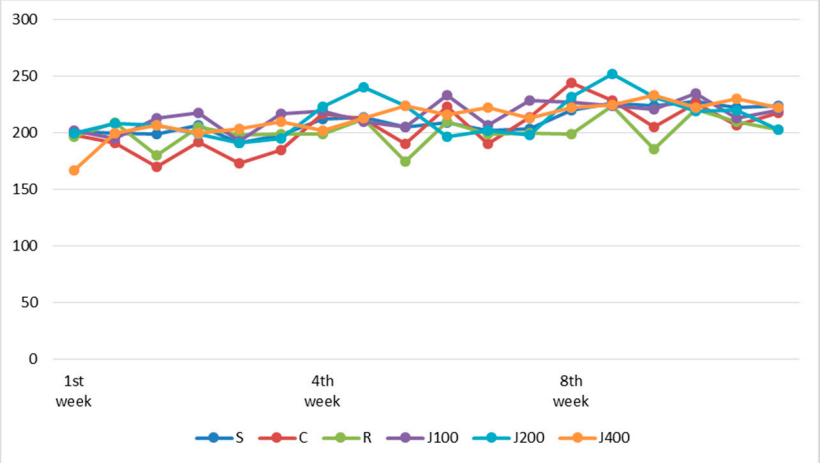


Figure 4. Body weight (g) changes in rats of the sham (S), control (C), reference (R), J100, J200, and J400 groups throughout the 8-week experimental period. The first, fourth, and eighth weeks are indicated on the x-axis for clarity.

The NMU-induced mammary tumor model was successfully established in all NMU-treated rats following a single intraperitoneal administration of 50 mg/kg NMU (Figure 5). Representative macroscopic images of the excised mammary tumors from the treatment groups are shown in Figure 6, illustrating the differences in tumor size among the experimental groups.

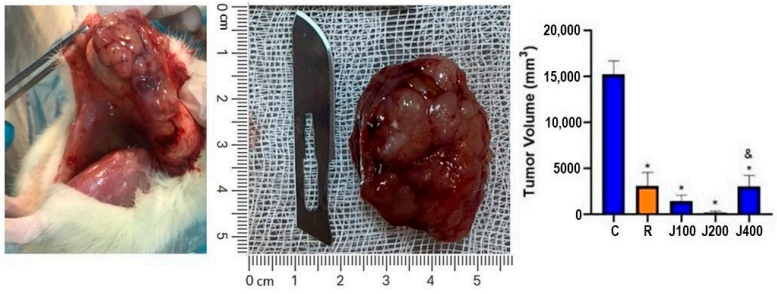


Figure 5. Post-treatment tumor volume assessment in rats with NMU-induced mammary tumors. C: Control; R: Reference; J100: *J. effusus* subsp. *effusus* sub-extract (100 mg/kg); J200: *J. effusus* subsp. *effusus* sub-extract (200 mg/kg); J400: *J. effusus* subsp. *effusus* sub-extract (400 mg/kg). * $p < 0.0001$, significantly different from C; $^{\&}$ $p < 0.05$, significantly different from J200 group.

The anticancer effects of *J. effusus* subsp. *effusus* extracts were subsequently evaluated in this model. Tumor volume measurements revealed pronounced differences among the experimental groups. The C group exhibited the highest mean tumor volume (15,232.70 ± 1464.00 mm^3). Treatment with *J. effusus* subsp. *effusus* extracts resulted in significant reductions in tumor volumes across all groups: R (3073.33 ± 1492.00 mm^3), J100 (1410.00 ± 689.00 mm^3), J200 (177.66 ± 165.00 mm^3), and J400 (3013.50 ± 1216.00 mm^3), with all groups showing statistically significant decreases compared to the control group ($p < 0.0001$). Among the treatment groups, the J200 group achieved the most pronounced suppression of tumor growth, which was significantly lower than both the C and the J400 groups ($p < 0.05$). No other statistically significant differences were observed among the remaining treatment groups.

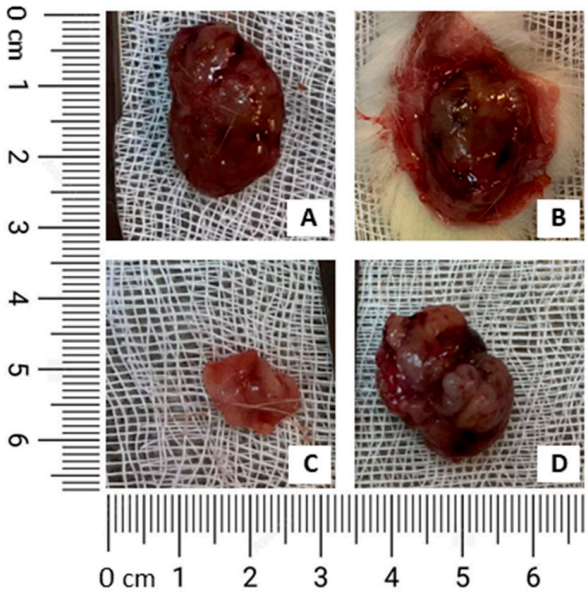


Figure 6. Representative macroscopic images of excised mammary tumors from each experimental group at the end of treatment. (**A**) Reference (R) group, (**B**) *J. effusus* subsp. *effusus* 100 mg/kg (J100), (**C**) *J. effusus* subsp. *effusus* 200 mg/kg (J200), (**D**) *J. effusus* subsp. *effusus* 400 mg/kg (J400). Note the markedly smaller tumor in the J200 group compared with the other groups, consistent with the tumor volume measurements.

3.3. Histopathological Results

Histopathological evaluation of mammary tissue sections demonstrated that the S group displayed preserved mammary gland architecture. The mammary gland exhibited well-defined terminal duct–lobular units with intact epithelial and myoepithelial cell layers supported by normal stromal tissue. Tumors graded using the Nottingham Histologic Score demonstrated a statistically significant difference in total score between the experimental groups. Histological analysis revealed that the C group displayed features of high-grade neoplasia, characterized by disorganized epithelial proliferation, significant nuclear atypia, and an elevated mitotic rate. Furthermore, the tumor microenvironment in this group was marked by dense lymphocytic infiltration and prominent stromal fibrosis (Figure 7).

Histopathological assessment based on the scoring system revealed a significant increase in tumor scores in all experimental groups compared to the S group ($p < 0.0001$). However, all treatment groups (R, J100, J200, and J400) exhibited significantly lower scores than the untreated C group ($p < 0.0001$). Among the treatment groups, the J400 group showed significantly higher scores than the J100 ($p < 0.05$) and J200 ($p < 0.0001$) groups. The tumor score in the J200 group demonstrated a histopathological pattern comparable to that observed in the R group (Figure 8).

Masson's Trichrome staining was performed to evaluate collagen deposition and fibrosis in mammary tissues. Quantitative analysis demonstrated markedly higher fibrosis in the C and R groups compared to the other groups (C: $p < 0.01$; R: $p < 0.05$). In contrast, the J100, J200, and J400 treatment groups exhibited significantly reduced collagen-positive areas compared with the C group (J100: $p < 0.001$; J200 and J400: $p < 0.0001$). Moreover, fibrosis levels were also significantly lower in the J100 ($p < 0.01$), J200 ($p < 0.0001$), and J400 ($p < 0.001$) groups compared with the R group (Figure 9).

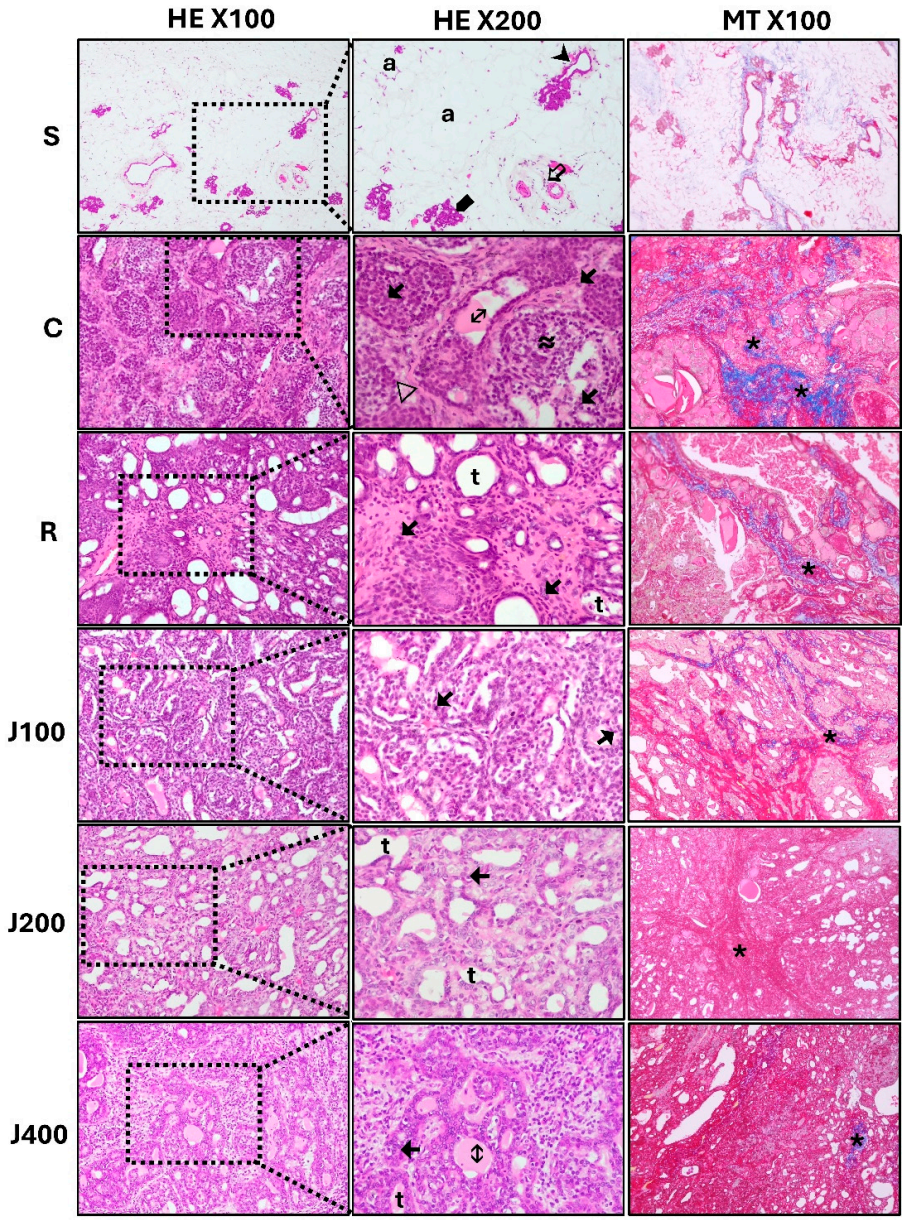


Figure 7. Representative histopathological images of mammary tissue sections from each experimental group. (a) Adipocyte, (➤) ductal epithelial cells, (⇨) blood vessels, (➡) intralobular secretory duct, (←) mitotic figure, (△) necrotic area, (↕) mucin accumulation in the ductal lumen, (≈) lymphocyte infiltration, (t) tubule, (*) collagen fibers. Masson's Trichrome (MT) staining revealed a normal and well-organized distribution of collagen fibers in the S group, whereas the C group exhibited markedly increased collagen deposition with a disorganized fiber pattern.

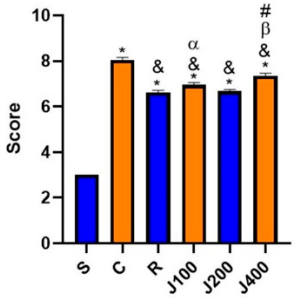


Figure 8. Histopathological grading of mammary tissues in rats at the end of the experimental period, evaluated using the Nottingham Grading System. S: Sham group; C: Control group; R: Reference group;

J100, J200, J400: *J. effusus* subsp. *effusus* ethyl acetate sub-extract (100, 200, and 400 mg/kg, respectively). * $p < 0.0001$ compared with the S group; $^{\&}$ $p < 0.0001$ compared with the C group; $^{\alpha}$ $p < 0.0001$ compared with the J400 group; $^{\beta}$ $p < 0.05$ compared with the J100 group; $^{\#}$ $p < 0.0001$ compared with the J200 group.

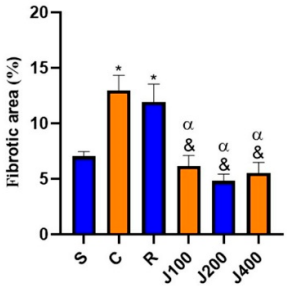


Figure 9. Quantitative analysis of fibrosis in mammary tissues based on the mean percentage of collagen-positive areas following Masson's Trichrome staining. S: Sham group; C: Control group; R: Reference group; J100, J200, J400: *J. effusus* subsp. *effusus* sub-extract (100, 200, and 400 mg/kg, respectively). * $p < 0.05$ compared with the S group; $^{\alpha}$ $p < 0.0001$ compared with the C group; $^{\&}$ $p < 0.001$ compared with the R group.

3.4. Immunohistochemical Findings

Immunohistochemical analyses were performed to evaluate the expression of ERα, HIF-1α, p53, and PCNA in mammary tumor tissues (Figure 10). ERα expression was highest in the C group, showing a significant increase compared with the S group ($p < 0.05$). Among the treatment groups, the J200 group displayed the lowest ERα immunoreactivity, with significantly reduced expression compared with the C, R, and J100 groups ($p < 0.05$). HIF-1α expression was elevated in the C group relative to the other groups. However, a statistically significant difference was detected only between the C and S groups ($p < 0.05$). Although HIF-1α levels tended to decrease in all treatment groups compared with the C group, these changes were not statistically significant ($p > 0.05$).

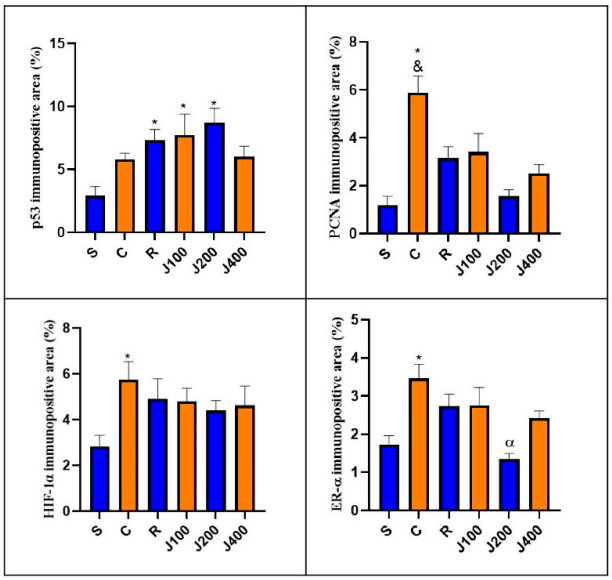


Figure 10. Quantitative analysis of immunopositive areas for p53, PCNA, HIF-1α, and ERα in mammary tissues. Data are expressed as mean ± SEM (n = 6). * $p < 0.05$, significant difference compared with the S group. $^{\&}$ $p < 0.05$, significant difference compared with the R, J100, J200, and J400 groups, $^{\alpha}$ $p < 0.05$, significant difference compared with the C, R, and J100 groups. S: Sham; C: Control, R: Reference, J100, J200, J400: *J. effusus* subsp. *effusus* ethyl acetate sub-extract at 100, 200, and 400 mg/kg, respectively.

p53 immunopositivity was minimal in the S group and markedly increased in all NMU-exposed groups. Significantly higher p53 expression was observed in the R, J100, and J200 groups compared with the S group ($p < 0.05$). PCNA expression was the highest in the C group and was significantly greater than that in the S group ($p < 0.05$). All treatment groups exhibited markedly reduced PCNA immunoreactivity compared with the C group ($p < 0.05$).

Representative immunohistochemical photomicrographs of ERα, HIF-1α, p53, and PCNA expression in the experimental groups are shown in Figure 11.

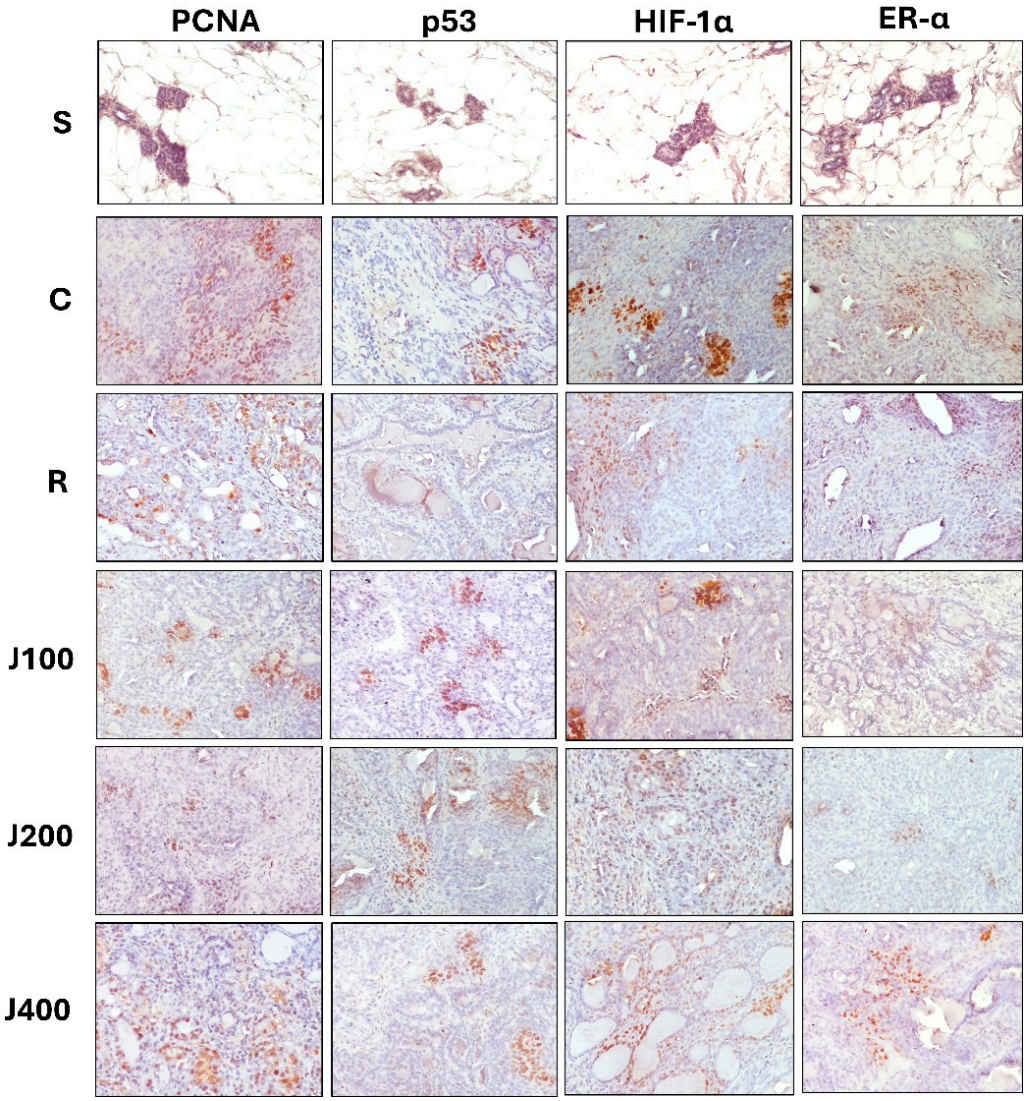


Figure 11. Representative immunohistochemical staining of mammary tumor tissues for PCNA, p53, HIF-1α, and ERα in rats (DAB chromogen, 3,3′-diaminobenzidine; hematoxylin counterstain; magnification ×200). Brown staining indicates immunopositive cells.

3.5. Comparative Analysis of ER-α and p53 Expressions

Significant differences in ERα and p53 mRNA expression levels were observed among the experimental groups (Table 4). The J100 and J200 groups exhibited significantly lower ERα expression levels compared with the R, C, J400, and S groups ($p < 0.05$). No significant differences were detected among the R, C, J400, and S groups. p53 mRNA expression was significantly reduced in the J100 and J200 groups compared with the R, J400, C, and S groups ($p < 0.05$). However, no significant differences were observed among the R, J400, C,

and S groups, although the R and J400 groups showed numerically higher median values than C and S.

Table 4. Expression levels of selected genes in experimental groups.

Groups	ERα	p53
	Median (Q1–Q3)	Median (Q1–Q3)
S	0.62 (0.23–3.41) [a]	0.98 (0.82–3.22) [a]
C	0.84 (0.73–1.28) [a]	1.01 (0.75–1.3) [a]
R	1.19 (0.15–20.82) [a]	1.94 (0.95–5.8) [a]
J100	0.08 (0.05–0.17) [b]	0.12 (0.08–0.34) [b]
J200	0.06 (0.03–0.12) [ab]	0.24 (0.03–0.39) [b]
J400	0.77 (0.61–1.39) [a]	2.17 (0.9–2.7) [a]

[a,b]: Different lowercase letters in the same column indicate statistically significant differences between the values ($p < 0.05$).

4. Discussion

The present study provides the first in vivo evidence that the ethyl acetate sub-extract of *J. effusus* subsp. *effusus* exerts antitumor activity in an NMU-induced rat mammary tumor model. The treatment with *J. effusus* subsp. *effusus* was associated with a marked reduction in tumor burden, improvement in histopathological tumor scores, attenuation of collagen deposition, and decreased PCNA immunoreactivity, indicating reduced proliferative activity within tumor tissues. Among the tested doses, 200 mg/kg of *J. effusus* subsp. *effusus* sub-extract produced the most consistent antitumor response, accompanied by lower ERα expression at both the protein and mRNA levels. In contrast, the weaker response observed at 400 mg/kg suggests a non-linear dose–response pattern rather than a simple dose-dependent effect. Although HIF-1α immunoreactivity showed only a non-significant tendency to decrease, and p53-related changes appeared more complex, these findings suggest that *J. effusus* subsp. *effusus* may influence multiple tumor-associated processes, including hormone receptor-related signaling, cellular proliferation, stromal remodeling, and stress-response pathways. Importantly, the comparable body weight gain among the experimental groups suggests that the treatments did not adversely affect the general health and growth of the animals during the study.

Recent phytochemical and pharmacological studies have demonstrated that species within the genus *Juncus* possess a wide range of biologically active secondary metabolites, including phenanthrene derivatives, flavonoids, and phenolic acids, which are associated with diverse pharmacological effects [7,11]. These compounds have shown antioxidant, anti-inflammatory, and antimicrobial properties, along with antiproliferative effects that are particularly relevant to their potential use against cancer [7,27,28].

Although these findings support the cytotoxic potential of *Juncus*-derived constituents, confirming their therapeutic value requires evidence from in vivo studies. In vitro studies of *Juncus* species have certainly deepened our understanding of how these constituents act. However, such models remain inherently limited in capturing the complexity of tumor progression in vivo. This limitation is not unique to *Juncus*-based research; rather, it reflects a broader translational challenge that is well-documented across cancer pharmacology. Conventional 2D cell cultures fail to adequately recapitulate the tumor microenvironment (TME), lacking critical three-dimensional cell–cell and cell–matrix interactions, stromal crosstalk, and systemic regulatory influences that are essential for disease progression [29,30].

This modeling gap is particularly consequential in hormone-dependent breast cancer, where estrogen receptor (ER) signaling is tightly regulated by both cell-autonomous and microenvironmental factors. The TME plays a central role in shaping ER-positive tumor behavior, yet conventional in vitro systems and many genetically engineered mouse models do not fully represent this biology, limiting their predictive utility [31]. These constraints contribute to the persistent discrepancies observed between preclinical efficacy and clinical outcomes [32].

Against this background, in vivo evaluation using the NMU-induced rat mammary tumor model represents a critical next step. This system closely recapitulates key features of human hormone-dependent breast carcinogenesis and estrogen-responsive tumor biology [33–35], making it a well-established model for translational research. In the present study, treatment with the ethyl acetate sub-extract of *J. effusus* subsp. *effusus*, a plant known for its phytoestrogenic properties, significantly suppressed tumor progression. This macroscopic effect was accompanied by coordinated molecular and histopathological changes, including downregulation of ER-α, HIF-1α, and PCNA expression, alongside improvements in parameters associated with tumor aggressiveness. These findings suggest that the antitumor response involves more than a single pathway, as discussed in detail below.

Regarding macroscopic tumor progression, tumor volume was reduced in all treatment groups, with the most pronounced effect observed in the J200 group. Notably, the highest dose (J400) was consistently less effective than the intermediate doses (J100 and J200), a pattern that was also reflected in the PCNA and ERα immunoreactivity results. This apparent non-monotonic dose–response relationship is not uncommon for plant-derived polyphenols and phytoestrogens, which frequently exhibit biphasic rather than linear dose–response behavior [36,37].

Several mechanisms may contribute to the reduced efficacy at the higher dose. First, the intestinal absorption and bioavailability of phenolic compounds can become saturated at higher doses, so that the increase in administered dose may not translate into a proportional increase in the effective tissue concentration [38,39]. Second, phenolic constituents that act as antioxidants at low-to-moderate concentrations may shift toward pro-oxidant or otherwise altered activity at higher concentrations, potentially contributing to the non-linear dose–response observed here [40,41]. Third, and particularly relevant in this ER-positive model, phytoestrogens can exert dose-dependent dual actions on estrogen receptor signaling, behaving as antagonists or weak modulators at lower concentrations while displaying estrogenic, proliferation-promoting activity at higher concentrations [42–44].

Regarding macroscopic tumor progression, the most pronounced reduction in tumor volume was observed in the J200 group, which was the only group to show a statistically significant decrease compared with the control. This finding was supported by the immunohistochemical results, as the J200 group exhibited the lowest ERα immunoreactivity together with the strongest tumor suppression, whereas the higher dose was associated with comparatively higher ERα expression and reduced efficacy. In ER-positive breast cancer, mammary gland proliferation and tumor growth are largely regulated through ER-α- and ER-β-mediated signaling pathways [45]. The tumor suppression observed at the effective dose (J200) may therefore be partly attributable to modulation of these hormonal pathways, while the non-linear dose–response pattern highlights the importance of dose optimization in future studies. However, in the absence of pharmacokinetic and bioavailability data, these mechanistic explanations remain speculative and warrant further investigation.

Tamoxifen, a selective estrogen receptor modulator, exerts its therapeutic effects primarily through competitive inhibition of ER-α, thereby altering downstream transcriptional programs within tumor cells. In hormone-dependent breast cancer models, including

NMU-induced mammary carcinogenesis, tamoxifen is widely used as a reference endocrine therapy due to its well-characterized modulation of estrogen receptor signaling pathways. Interestingly, several studies have reported increased ERα gene expression in tumors that respond favorably to tamoxifen treatment [46,47].

In the present study, the tamoxifen-treated group showed maintained or slightly elevated ERα mRNA expression, while ERα protein levels were reduced compared with the tumor control group. This dissociation between mRNA and protein is well-established in the antiestrogen literature. Studies examining antiestrogen effects on breast tumors and cell lines consistently report this same pattern, where mRNA persists despite protein depletion [48,49]. Tamoxifen likely destabilizes the receptor protein while also triggering compensatory transcriptional activity, although the underlying mechanism remains to be fully elucidated.

J. effusus subsp. *effusus* extract behaved differently, lowering both ERα mRNA and protein together. The strongest suppression at both levels came from the J200 dose, the same one that produced the greatest reduction in tumor volume. This coordinated downregulation differs markedly from the tamoxifen pattern, suggesting a fundamentally different mode of action on estrogen receptor regulation. The ability of *J. effusus* subsp. *effusus* to target ER-α at both transcript and protein levels indicates it acts on a core control point in receptor synthesis and degradation. Whether this reflects the activity of individual bioactive compounds or synergistic effects of multiple constituents warrants further investigation. These findings support the potential of *J. effusus* subsp. *effusus* as a candidate therapy in ER-positive breast cancer, particularly for understanding how its active constituents modulate estrogen receptor signaling in hormone-responsive tumors.

In experimental rat models of mammary tumors, histopathological scoring systems are widely used to assess disease severity and therapeutic response. These systems integrate multiple parameters, including mitotic index, nuclear atypia, tubule formation, and stromal fibrosis, thereby providing a standardized and reproducible framework for tumor grading. Consistent with previous studies [50,51], NMU-induced mammary tumors typically exhibit elevated histopathological scores, reflecting increased tumor aggressiveness. In the present study, treatment with *J. effusus* subsp. *effusus* sub-extracts improved several histopathological features, in line with reduced tumor progression. Among the treatment groups, the J200 dose showed the most notable effects, characterized by decreased mitotic activity, reduced nuclear atypia, and attenuation of stromal remodeling. Masson's Trichrome staining reinforced this picture, revealing markedly reduced collagen deposition across all *J. effusus* subsp. *effusus* treatment groups compared with both control and tamoxifen groups. This parallel decline in fibrosis suggests that the extract's antitumor effects extend beyond cell proliferation to include suppression of the stromal remodeling that often accompanies aggressive tumor growth. Overall, the improvements in tissue architecture and the reduction in proliferative markers suggest that J. effusus subsp. *effusus* treatment exerted beneficial effects on tumor progression. The J200 dose emerged as the most effective, making it a promising candidate for further development as a plant-derived antitumor agent in hormone-responsive breast cancer. Further work is needed to understand how *J. effusus* subsp. *effusus* affects tumor progression and to identify which of its constituents are responsible for these effects.

For evaluation of tumor cell proliferation, PCNA expression was assessed to further characterize the proliferative status of the tumor tissues. PCNA is a nuclear protein involved in DNA replication and repair and serves as a well-established marker of cellular proliferation, offering insight into tumor growth dynamics and treatment response [52,53]. Reduced PCNA expression following therapeutic intervention is generally taken as a sign of decreased tumor cell proliferation and a corresponding antiproliferative effect, and

immunohistochemical assessment of PCNA is routinely used in both in vitro and in vivo cancer models to evaluate candidate anticancer agents [54,55].

In the present study, tumor-bearing groups showed elevated PCNA expression compared with the sham group, reflecting the proliferative nature of mammary carcinoma. Treatment with *J. effusus* subsp. *effusus* extract reduced PCNA expression across all tested doses relative to control, indicating a clear antiproliferative effect. The J200 group exhibited the lowest PCNA levels numerically, though this difference did not reach statistical significance compared with the other treatment groups. These findings highlight the preclinical relevance of *J. effusus* subsp. *effusus* and confirm PCNA as a meaningful indicator of treatment response in this tumor model. Estrogen signaling drives mammary epithelial proliferation, and the fact that both PCNA and ERα declined together following *J. effusus* subsp. *effusus* treatment suggests that part of its antiproliferative action may occur through suppression of estrogen receptor-mediated signaling.

HIF-1α is frequently upregulated as breast cancer progresses, and its overexpression has long been linked to poor prognosis—not surprising, given its central role in driving angiogenesis, metabolic adaptation, invasion, and resistance to therapy [56]. Large-scale meta-analyses back up this trend. Elevated HIF-1α expression keeps showing up alongside shorter survival, disease-free survival, and relapse-free survival, as well as more aggressive disease features like higher tumor grade, lymph node involvement, and ER-negative status. Individual cohort studies tell a similar story. In lymph node-positive breast cancer specifically, HIF-1α overexpression has repeatedly been linked to worse survival outcomes [57,58]. HIF-1α, in short, is one of the more consistent markers of tumor hypoxia and aggressive disease behavior.

In the present study, HIF-1α immunoreactivity was higher in the control group than in the sham group, consistent with active hypoxia-associated signaling within the mammary tumors. Differences among the treatment groups did not reach statistical significance, though a general trend toward lower HIF-1α expression followed *J. effusus* subsp. *effusus* administration. This could reflect a partial easing of hypoxia-related signaling and a reduced need for adaptive responses within the tumor microenvironment. Because HIF-1α drives both angiogenesis and metabolic reprogramming, even a modest drop in its expression could still matter biologically. A similar effect has been reported for other natural compounds in breast cancer models [59,60], raising the possibility that the phenolic constituents in this extract act through a comparable route. These findings remain preliminary, but they point to the possibility that *J. effusus* subsp. *effusus* contributes to the modulation of hypoxia-associated signaling pathways. Further work is needed to clarify how *J. effusus* subsp. *effusus* treatment relates to HIF-1α-mediated responses in mammary tumors.

In addition to estrogen receptor modulation, the tumor suppressor gene p53 plays a central role in regulating cell cycle progression and maintaining genomic integrity by coordinating cellular responses to stress and apoptosis. In ER-positive breast cancer, p53 signaling is frequently altered, and carcinogen-induced models such as NMU are known to promote p53 dysregulation, including the accumulation of dysfunctional protein forms with impaired tumor-suppressive activity [61–63].

In the present study, p53 protein levels were markedly elevated in the R, J100, and J200 treatment groups compared with the sham group, whereas the C group showed intermediate p53 expression that did not differ significantly from any other group. This elevation of p53 in treated groups is consistent with NMU-induced tumorigenesis, where p53 mutations commonly lead to stabilization of dysfunctional protein, a pattern well-documented in carcinogen-induced mammary tumor models [63]. At the same time, p53 mRNA levels fell significantly in the J100 and J200 groups relative to the other experimental groups, so the transcript and protein levels were clearly moving in opposite directions. When p53

mRNA drops but protein stays high, the explanation usually lies after transcription, in how the protein is stabilized or cleared. Impaired degradation, for instance, can let p53 build up and persist even as its mRNA declines [64]. Because p53 protein abundance is regulated at multiple levels, including MDM2-mediated degradation [65], mutation-related stabilization [63], and post-translational modifications [66], understanding what is actually happening requires looking at both mRNA and protein together. This dual assessment provides a more complete picture of p53 regulation in this context.

The persistence of elevated p53 protein despite reduced p53 mRNA in the J100 and J200 groups indicates that *J. effusus* subsp. *effusus* does not suppress p53 simply by reducing how much of the gene gets transcribed. Instead, the antitumor effects we observed in this study likely operate through different routes that do not depend on lowering p53 levels. Whether the accumulated p53 represents functional tumor suppression or reflects the nonfunctional protein forms typical of NMU-induced tumors remains an open question. Clarifying this would require additional work, such as checking for p53 mutations or measuring whether the p53 that is present is actually active. These findings highlight how complex p53 regulation becomes in carcinogen-induced tumors and suggest that future studies should combine both expression analysis and functional validation to get a complete picture.

In the present study, the phenolic composition of the *J. effusus* subsp. *effusus* ethyl acetate sub-extract was characterized by UHPLC-ESI-MS/MS, which revealed a chemically diverse profile comprising quinic acid, chlorogenic acid, peonidin-3-*O*-glucoside, 4-Hydroxybenzoic acid, ferulic acid, *p*-coumaric acid, luteolin, and apigenin. Of these, 4-Hydroxybenzoic acid, chlorogenic acid, and ferulic acid emerged as the predominant constituents. This composition aligns with earlier reports identifying hydroxycinnamic acid derivatives and flavonoids as the dominant chemical classes in *J. effusus*, whereas phenanthrene-type metabolites appear to be largely confined to alternative extraction systems and fractions [27,67].

Several of the identified compounds—including luteolin, chlorogenic acid, gallic acid, ferulic acid, *p*-coumaric acid, apigenin, and peonidin-3-*O*-glucoside—have established links to anticancer activity in breast cancer and other tumor models. Luteolin, in particular, is among the most extensively characterized constituents in this regard and has been reported to suppress tumor growth through apoptosis induction, oxidative stress modulation, and cell cycle arrest. In mammary carcinoma models, luteolin treatment has been shown to reduce tumor burden while enhancing antioxidant defenses and promoting apoptotic activity [68]. Chlorogenic acid has likewise been reported to inhibit proliferation, invasion, and epithelial–mesenchymal transition progression, partly through suppression of NF-κB signaling, while also enhancing antitumor immune responses in breast cancer models [69,70].

The remaining compounds identified in the extract have been investigated less extensively, yet the available evidence suggests that they may also contribute to the observed antitumor effects. Ferulic acid, *p*-coumaric acid, gallic acid, apigenin, and 4-Hydroxybenzoic acid have relatively limited direct evidence from in vivo cancer models. However, studies across different tumor systems have demonstrated their capacity to modulate processes closely linked to tumor progression, including oxidative stress, cell-cycle regulation, angiogenesis, and metastatic signaling [71,72]. The concurrent reductions in ER-α, HIF-1α, and PCNA expression observed in the treated groups are unlikely to be explained by the activity of a single constituent alone. Instead, these changes may reflect the combined actions of multiple phenolic compounds acting on interconnected pathways involved in estrogen signaling, adaptation to hypoxia, and cellular proliferation. Such complementary effects could help explain the suppression of tumor growth observed in the present study.

Several limitations should be considered when interpreting these findings. The lower efficacy observed at 400 mg/kg suggests a non-linear dose–response relationship that cannot be fully explained in the absence of pharmacokinetic and bioavailability data. In addition, the HIF-1α and p53 findings should be interpreted with caution, since the panel of molecular markers examined here was relatively narrow and does not allow firm conclusions about the pathways involved. Broader molecular profiling, combined with pharmacokinetic characterization, would help clarify how *J. effusus* exerts its antitumor activity.

5. Conclusions

The present study demonstrates that the ethyl acetate sub-extract of *Juncus effusus* subsp. *effusus* exerts antitumor effects in an NMU-induced rat mammary tumor model, with the most pronounced response observed at 200 mg/kg. This effect was supported by reduced tumor burden, improved histopathological scores, decreased collagen deposition, and lower PCNA and ERα expression. Still, the broader pattern of results suggests that *J. effusus* subsp. *effusus* may modulate multiple processes involved in tumor progression. Nevertheless, these findings provide a preclinical basis for further investigation of *J. effusus* and its phenolic constituents in hormone-responsive mammary tumor models.

Supplementary Materials: The following supporting information can be downloaded at https://www.mdpi.com/article/10.3390/molecules31152581/s1. Figure S1: MRM chromatograms of the ethyl acetate sub-extract of *J. effusus* subsp. *effusus*; Table S1: MRM transitions, and MS/MS parameters of the UHPLC-ESI-MS/MS method.

Author Contributions: Conceptualization, İ.E., M.A.D. and O.O.Ş.; Methodology, M.A.D., S.Ö.A.D. and İ.S.; Investigation, İ.E. and M.A.D.; Data Curation, İ.S., O.T. and K.T.; Formal analysis, İ.E., M.A.D., İ.S., S.Ö.A.D., O.T. and K.T.; Writing—Original Draft Preparation, İ.E., M.A.D. and İ.S.; Writing—Review & Editing, İ.E. and O.O.Ş. All authors have read and agreed to the published version of the manuscript.

Funding: This research was funded by the Ankara University Scientific Research Projects Coordination Office (Project No. 2505, Project Code: TSA-2022-2505).

Institutional Review Board Statement: The study was approved by the Gazi University Local Ethics Committee for Animal Experiments (Decision date: 27 April 2022, Approval number: G.Ü.ET-22.054).

Informed Consent Statement: Not applicable.

Data Availability Statement: Data will be made available upon request.

Conflicts of Interest: The authors declare no conflicts of interest.

References

1. Albers, F.E.M.; Lou, M.W.C.; Dashti, S.G.; Swain, C.T.V.; Rinaldi, S.; Viallon, V.; Karahalios, A.; Brown, K.A.; Gunter, M.J.; Milne, L.; et al. Sex-steroid hormones and risk of postmenopausal estrogen receptor-positive breast cancer: A case–cohort analysis. *Cancer Causes Control.* **2024**, *35*, 921–933. [CrossRef] [PubMed]
2. Giaquinto, A.N.; Sung, H.; Miller, K.D.; Kramer, J.L.; Newman, L.A.; Minihan, A.; Jemal, A.; Siegel, R.L. Breast cancer statistics, 2022. *CA Cancer J. Clin.* **2022**, *72*, 524–541. [CrossRef] [PubMed]
3. Jeselsohn, R.; Buchwalter, G.; De Angelis, C.; Brown, M.; Schiff, R. ESR1 mutations—A mechanism for acquired endocrine resistance in breast cancer. *Nat. Rev. Clin. Oncol.* **2015**, *12*, 573–583. [CrossRef] [PubMed]
4. Slanar, O.; Hronova, K.; Bartosova, O.; Sima, M. Recent advances in the personalized treatment of estrogen receptor-positive breast cancer with tamoxifen: A focus on pharmacogenomics. *Expert Opin. Drug Metab. Toxicol.* **2021**, *17*, 307–321. [CrossRef] [PubMed]
5. Tommasi, C.; Balsano, R.; Corianò, M.; Pellegrino, B.; Saba, G.; Bardanzellu, F.; Denaro, N.; Ramundo, M.; Toma, I.; Fusaro, A.; et al. Long-term effects of breast cancer therapy and care: Calm after the storm? *J. Clin. Med.* **2022**, *11*, 7239. [CrossRef] [PubMed]
6. Kim, Y.J.; Park, C.I.; Park, J.S.; Ahn, E.M. Antioxidant and cytotoxic activity of compounds from the stem of *Juncus effusus*. *J. Appl. Biol. Chem.* **2014**, *57*, 47–51. [CrossRef]

7. El-Shamy, A.I.; Abdel-Razek, A.F.; Nassar, M.I. Phytochemical review of *Juncus* L. genus (Fam. Juncaceae). *Arab. J. Chem.* **2015**, *8*, 614–623. [CrossRef]
8. Stefko, D.; Kusz, N.; Barta, A.; Kele, Z.; Bakacsy, L.; Szepesi, A.; Fazakas, C.; Wilhelm, I.; Krizbai, I.A.; Hohmann, J.; et al. Gerardiins A–L and structurally related phenanthrenes from the halophyte plant *Juncus gerardii* and their cytotoxicity against triple-negative breast cancer cells. *J. Nat. Prod.* **2020**, *83*, 3058–3068. [CrossRef] [PubMed]
9. Kuo, C.Y.; Schelz, Z.; Toth, B.; Vasas, A.; Ocsovszki, I.; Chang, F.R.; Hohmann, J.; Zupko, I.; Wang, H.C. Investigation of natural phenanthrenes and the antiproliferative potential of juncusol in cervical cancer cell lines. *Phytomedicine* **2019**, *58*, 152770. [CrossRef] [PubMed]
10. Kusz, N.; Stefko, D.; Barta, A.; Kincses, A.; Szemeredi, N.; Spengler, G.; Hohmann, J.; Vasas, A. Juncaceae species as promising sources of phenanthrenes: Antiproliferative compounds from *Juncus maritimus* Lam. *Molecules* **2021**, *26*, 999. [CrossRef] [PubMed]
11. Bus, C.; Stefko, B.T.; Hohmann, J.; Vasas, A. Family Juncaceae: Promising source of biologically active natural phenanthrenes. *Phytochem. Rev.* **2018**, *17*, 833–851. [CrossRef]
12. Güler, N. *Vizenin Flora ve Vejetasyonu*; Orman Genel Müdürlüğü: Ankara, Türkiye, 2025. Available online: https://www.ogm.gov.tr/sertifikasyon/istanbul/V%C4%B0ZE%20FLORASI%20.pdf (accessed on 5 December 2025).
13. Güner, Ö.; Akçiçek, E. Ulus Dağı'nın (Balıkesir-Türkiye) endemik ve nadir bitkileri. *Bağbahçe Bilim Derg.* **2014**, *1*, 32–38. [CrossRef]
14. Liu, Y.; Ma, H.; Yao, J. ERα, a key target for cancer therapy: A review. *Onco Targets Ther.* **2020**, *13*, 2183–2191. [CrossRef] [PubMed]
15. Osborne, C.K.; Schiff, R.; Fuqua, S.A.; Shou, J. Estrogen receptor: Current understanding of its activation and modulation. *Clin. Cancer Res.* **2001**, *7*, 4338s–4342s. [PubMed]
16. Hafner, A.; Bulyk, M.L.; Jambhekar, A.; Lahav, G. The multiple mechanisms that regulate p53 activity and cell fate. *Nat. Rev. Mol. Cell Biol.* **2019**, *20*, 199–210. [CrossRef] [PubMed]
17. Choe, K.N.; Moldovan, G.L. Forging ahead through darkness: PCNA, still the principal conductor at the replication fork. *Mol. Cell* **2017**, *65*, 380–392. [CrossRef] [PubMed]
18. Semenza, G.L. Defining the role of hypoxia-inducible factor 1 in cancer biology and therapeutics. *Oncogene* **2010**, *29*, 625–634. [CrossRef] [PubMed]
19. Snogerup, S. *Juncus*. In *Flora of Turkey and the East Aegean Islands*; Davis, P.H., Ed.; Edinburgh University Press: Edinburgh, UK, 1985; Volume 9, pp. 1–25.
20. Güner, A. Juncaceae. In *Türkiye Bitkileri Listesi (Damarlı Bitkiler)*; Güner, A., Aslan, S., Ekim, T., Vural, M., Babaç, M.T., Eds.; Nezahat Gökyiğit Botanik Bahçesi ve Flora Araştırmaları Derneği Yayını: İstanbul, Türkiye, 2012; pp. 542–545.
21. Can, H.; Güven, L.; Demirkaya Miloğlu, F.; Abd El-Aty, A.M. Development and validation of a UHPLC-ESI-MS/MS method for the simultaneous determination of organic acids and phenolic compounds in *Filipendula vulgaris*, *Polygonum divaricatum*, *Hypericum linarioides*, and *Rheum ribes*. *Microchem. J.* **2024**, *201*, 110683. [CrossRef]
22. Belobrajdic, D.P.; McIntosh, G.H. Dietary butyrate inhibits NMU-induced mammary cancer in rats. *Nutr. Cancer* **2000**, *36*, 217–223. [CrossRef] [PubMed]
23. Direcks, W.G.E.; Gelder, M.; Lammertsma, A.A.; Molthoff, C.F.M. A new rat model of human breast cancer for evaluating efficacy of new anti-cancer agents in vivo. *Cancer Biol. Ther.* **2008**, *7*, 532–537. [CrossRef] [PubMed]
24. Elston, C.W.; Ellis, I.O. Pathological prognostic factors in breast cancer. I. The value of histological grade in breast cancer: Experience from a large study with long-term follow-up. *Histopathology* **1991**, *19*, 403–410. [CrossRef] [PubMed]
25. Metcalf, K.J.; Hayward, M.K.; Berens, E.; Ironside, A.J.; Stashko, C.; Hwang, E.S.; Weaver, V.M. Immunosuppressive glycoproteins are associated with breast tumor fibrosis and aggression. *Matrix Biol. Plus* **2022**, *14*, 100105. [CrossRef] [PubMed]
26. Santana-Krímskaya, S.E.; Franco-Molina, M.A.; Zárate-Triviño, D.G.; Prado-Garcia, H.; Zapata-Benavides, P.; Torres-Del-Muro, F.; Rodriguez-Padilla, C. IMMUNEPOTENT CRP plus doxorubicin/cyclophosphamide chemotherapy remodel the tumor microenvironment in an air pouch triple-negative breast cancer murine model. *Biomed. Pharmacother.* **2020**, *126*, 110062. [CrossRef] [PubMed]
27. Ma, W.; Ding, Y.Y.; Liu, F.; Zhang, Y.; Li, N. Cytotoxic and anti-inflammatory constituents from *Juncus effusus*. *J. Mex. Chem. Soc.* **2016**, *60*, 83–88.
28. Liao, Y.J.; Zhai, H.F.; Zhang, B.; Duan, T.X.; Huang, J.M. Anxiolytic and sedative effects of dehydroeffusol from *Juncus effusus* in mice. *Planta Med.* **2011**, *77*, 416–420. [CrossRef] [PubMed]
29. Das, V.; Bruzzese, F.; Konečný, P.; Iannelli, F.; Budillon, A.; Hajduch, M. Pathophysiologically relevant in vitro tumor models for drug screening. *Drug Discov. Today* **2015**, *20*, 848–855. [CrossRef] [PubMed]
30. Asghar, W.; El Assal, R.; Shafiee, H.; Pitteri, S.; Paulmurugan, R.; Demirci, U. Engineering cancer microenvironments for in vitro 3-D tumor models. *Mater. Today* **2015**, *18*, 539–553. [CrossRef] [PubMed]
31. Özdemir, B.C.; Sflomos, G.; Brisken, C. The challenges of modeling hormone receptor-positive breast cancer in mice. *Endocr.-Relat. Cancer* **2018**, *25*, R319–R330. [CrossRef] [PubMed]

32. Sflomos, G.; Dormoy, V.; Metsalu, T.; Jeitziner, R.; Battista, L.; Scabia, V.; Raffoul, W.; Delaloye, J.F.; Treboux, A.; Fiche, M.; et al. A preclinical model for ERα-positive breast cancer points to the epithelial microenvironment as determinant of luminal phenotype and hormone response. *Cancer Cell* **2016**, *29*, 407–422. [CrossRef] [PubMed]
33. Chan, M.M.; Lu, X.; Merchant, F.M.; Iglehart, J.D.; Miron, P.L. Serial transplantation of NMU-induced rat mammary tumors: A model of human breast cancer progression. *Int. J. Cancer* **2007**, *121*, 474–485. [CrossRef] [PubMed]
34. Milton, J.D.; Jose, M.A. Anticancer activity of ethyl acetate root extract of Xanthium strumarium Linn. in N-nitroso N-methyl urea induced mammary carcinoma in female Sprague-Dawley rats. *Res. J. Pharm. Technol.* **2016**, *9*, 1115. [CrossRef]
35. Yaacob, N.S.Y.; Yankuzo, H.M.Y.; Devaraj, S.D.; Wong, K.; Lai, C.S. Anti-tumor action, clinical biochemistry profile and phytochemical constituents of a pharmacologically active fraction of S. crispus in NMU-induced rat mammary tumour model. *PLoS ONE* **2015**, *10*, e0126426. [CrossRef] [PubMed]
36. Jodynis-Liebert, J.; Kujawska, M. Biphasic dose-response induced by phytochemicals: Experimental evidence. *J. Clin. Med.* **2020**, *9*, 718. [CrossRef] [PubMed]
37. Calabrese, E.J.; Mattson, M.P.; Calabrese, V. Dose response biology: The case of resveratrol. *Hum. Exp. Toxicol.* **2010**, *29*, 1034–1037. [CrossRef] [PubMed]
38. Rodriguez-Mateos, A.; Feliciano, R.P.; Cifuentes-Gomez, T.; Spencer, J.P. Bioavailability of wild blueberry (poly) phenols at different levels of intake. *J. Berry Res.* **2016**, *6*, 137–148. [CrossRef]
39. Scholz, S.; Williamson, G. Interactions affecting the bioavailability of dietary polyphenols in vivo. *Int. J. Vitam. Nutr. Res.* **2007**, *77*, 224–235. [CrossRef] [PubMed]
40. Stepanic, V.; Gasparovic, A.C.; Troselj, K.G.; Amic, D.; Zarkovic, N. Selected attributes of polyphenols in targeting oxidative stress in cancer. *Curr. Top. Med. Chem.* **2015**, *15*, 496–509. [CrossRef] [PubMed]
41. Vrankova, S.; Cebova, M.; Klimentova, J.; Pechanova, O. Redox Paradox of Polyphenols: Bioavailability, Hormesis, and Safety Concerns. *Phytother. Res.* **2026**, *40*, 2437–2455. [CrossRef] [PubMed]
42. Maggiolini, M.; Bonofiglio, D.; Marsico, S.; Panno, M.L.; Cenni, B.; Picard, D.; Andò, S. Estrogen receptor alpha mediates the proliferative but not the cytotoxic dose-dependent effects of two major phytoestrogens on human breast cancer cells. *Mol. Pharmacol.* **2001**, *60*, 595–602. [CrossRef] [PubMed]
43. Leclercq, G.; Jacquot, Y. Interactions of isoflavones and other plant derived estrogens with estrogen receptors for prevention and treatment of breast cancer-considerations concerning related efficacy and safety. *J. Steroid Biochem. Mol. Biol.* **2014**, *139*, 237–244. [CrossRef] [PubMed]
44. Bilal, I.; Chowdhury, A.; Davidson, J.; Whitehead, S. Phytoestrogens and prevention of breast cancer: The contentious debate. *World J. Clin. Oncol.* **2014**, *5*, 705–712. [CrossRef] [PubMed]
45. Wang, X.; Zhang, N.; Huo, Q.; Sun, M.; Lv, S.; Yang, Q. Huaier aqueous extract suppresses human breast cancer cell proliferation through inhibition of estrogen receptor α signaling. *Int. J. Oncol.* **2013**, *43*, 321–328. [CrossRef] [PubMed]
46. Frasor, J.; Chang, E.C.; Komm, B.; Lin, C.Y.; Vega, V.B.; Liu, E.T.; Miller, L.D.; Smeds, J.; Bergh, J.; Katzenellenbogen, B.S. Gene expression preferentially regulated by tamoxifen in breast cancer cells and correlations with clinical outcome. *Cancer Res.* **2006**, *66*, 7334–7340. [CrossRef] [PubMed]
47. Kim, C.; Tang, G.; Pogue-Geile, K.L.; Costantino, J.P.; Baehner, F.L.; Baker, J.; Cronin, M.T.; Watson, D.; Shak, S.; Bohn, O.L.; et al. Estrogen receptor (ESR1) mRNA expression and benefit from tamoxifen in the treatment and prevention of estrogen receptor–positive breast cancer. *J. Clin. Oncol.* **2011**, *29*, 4160–4167. [CrossRef] [PubMed]
48. McClelland, R.A.; Manning, D.L.; Gee, J.M.; Anderson, E.; Clarke, R.; Howell, A.; Dowsett, M.; Robertson, J.F.R.; Blamey, R.W.; Wakeling, A.E.; et al. Effects of short-term antiestrogen treatment of primary breast cancer on estrogen receptor mRNA and protein expression and on estrogen-regulated genes. *Breast Cancer Res. Treat.* **1996**, *41*, 31–41. [CrossRef] [PubMed]
49. Pink, J.J.; Jordan, V.C. Models of estrogen receptor regulation by estrogens and antiestrogens in breast cancer cell lines. *Cancer Res.* **1996**, *56*, 2321–2330. [PubMed]
50. Alvarado, A.; Lopes, A.C.; Faustino-Rocha, A.I.; Cabrita, A.M.S.; Ferreira, R.; Oliveira, P.A.; Colaço, B. Prognostic factors in MNU and DMBA-induced mammary tumors in female rats. *Pathol. Res. Pract.* **2017**, *213*, 441–446. [CrossRef] [PubMed]
51. Perse, M.; Cerar, A.; Injac, R.; Štrukelj, B. N-methylnitrosourea induced breast cancer in rat, the histopathology of the resulting tumors and its drawbacks as a model. *Pathol. Oncol. Res.* **2009**, *15*, 115–121. [CrossRef] [PubMed]
52. Moldovan, G.L.; Pfander, B.; Jentsch, S. PCNA, the maestro of the replication fork. *Cell* **2007**, *129*, 665–679. [CrossRef] [PubMed]
53. Malkas, L.H.; Herbert, B.S.; Abdel-Aziz, W.; Dobrolecki, L.E.; Liu, Y.; Agarwal, B.; Hoelz, D.; Badve, S.; Schnaper, L.; Arnold, R.J.; et al. A cancer-associated PCNA expressed in breast cancer has implications as a potential biomarker. *Proc. Natl. Acad. Sci. USA* **2006**, *103*, 19472–19477. [CrossRef] [PubMed]
54. Korak, T.; Ayaz, H.; Aşır, F. Skimmianine modulates tumor proliferation and immune dynamics in breast cancer by targeting PCNA and TNF-α. *Pharmaceuticals* **2025**, *18*, 756. [CrossRef] [PubMed]
55. Yu, C.C.W.; Woods, A.L.; Levison, D.A. The assessment of cellular proliferation by immunohistochemistry: A review of currently available methods and their applications. *Histochem. J.* **1992**, *24*, 121–131. [CrossRef] [PubMed]

56. Vleugel, M.M.; Greijer, A.E.; Shvarts, A.; van der Groep, P.; van Berkel, M.; Aarbodem, Y.; van Tinteren, H.; Harris, A.L.; van Diest, P.J.; van der Wall, E. Differential prognostic impact of hypoxia induced and diffuse HIF-1α expression in invasive breast cancer. *J. Clin. Pathol.* **2005**, *58*, 172–177. [CrossRef] [PubMed]
57. Schindl, M.; Schoppmann, S.F.; Samonigg, H.; Hausmaninger, H.; Kwasny, W.; Gnant, M.; Jakesz, R.; Kubista, E.; Birner, P.; Oberhuber, G. Overexpression of hypoxia-inducible factor 1α is associated with an unfavorable prognosis in lymph node-positive breast cancer. *Clin. Cancer Res.* **2002**, *8*, 1831–1837. [PubMed]
58. Yamamoto, Y.; Ibusuki, M.; Okumura, Y.; Kawasoe, T.; Kai, K.; Iyama, K.; Iwase, H. Hypoxia-inducible factor 1α is closely linked to an aggressive phenotype in breast cancer. *Breast Cancer Res. Treat.* **2008**, *110*, 465–475. [CrossRef] [PubMed]
59. Su, Q.; Wang, J.; Wu, Q.; Ullah, A.; Ghauri, M.A.; Sarwar, A.; Chen, L.; Liu, F.; Zhang, Y. Sanguinarine combats hypoxia-induced activation of EphB4 and HIF-1α pathways in breast cancer. *Phytomedicine* **2021**, *84*, 153503. [CrossRef] [PubMed]
60. Liu, Y.; Veena, C.K.; Morgan, J.B.; Mohammed, K.A.; Jekabsons, M.B.; Nagle, D.G.; Zhou, Y.D. Methylalpinumisoflavone inhibits hypoxia-inducible factor-1 (HIF-1) activation by simultaneously targeting multiple pathways. *J. Biol. Chem.* **2009**, *284*, 5859–5868. [CrossRef] [PubMed]
61. Marvalim, C.; Datta, A.; Lee, S.C. Role of p53 in breast cancer progression: An insight into p53 targeted therapy. *Theranostics* **2023**, *13*, 1421–1442. [CrossRef] [PubMed]
62. Qayoom, H.; Ul Haq, B.; Sofi, S.; Jan, N.; Jan, A.; Mir, M.A. Targeting mutant p53: A key player in breast cancer pathogenesis and beyond. *Cell Commun. Signal.* **2024**, *22*, 484. [CrossRef] [PubMed]
63. Umekita, Y.; Kobayashi, K.; Saheki, T.; Yoshida, H. Nuclear accumulation of p53 protein correlates with mutations in the p53 gene on archival paraffin-embedded tissues of human breast cancer. *Jpn. J. Cancer Res.* **1994**, *85*, 825–830. [CrossRef] [PubMed]
64. Bode, A.M.; Dong, Z. Post-translational modification of p53 in tumorigenesis. *Nat. Rev. Cancer* **2004**, *4*, 793–805. [CrossRef] [PubMed]
65. Kubbutat, M.H.G.; Jones, S.N.; Vousden, K.H. Regulation of p53 stability by Mdm2. *Nature* **1997**, *387*, 299–303. [CrossRef] [PubMed]
66. Harris, S.L.; Levine, A.J. The p53 pathway: Positive and negative feedback loops. *Oncogene* **2005**, *24*, 2899–2908. [CrossRef] [PubMed]
67. Ishiuchi, K.; Kosuge, Y.; Hamagami, H.; Ozaki, M.; Ishige, K.; Ito, Y.; Kitanaka, S. Chemical constituents isolated from *Juncus effusus* induce cytotoxicity in HT22 cells. *J. Nat. Med.* **2015**, *69*, 421–426. [CrossRef] [PubMed]
68. Samy, R.P.; Gopalakrishnakone, P.; Ignacimuthu, S. Anti-tumor promoting potential of luteolin against 7,12-dimethylbenz(a)anthracene-induced mammary tumors in rats. *Chem. Biol. Interact.* **2006**, *164*, 1–14. [CrossRef] [PubMed]
69. Xue, W.; Hao, J.; Zhang, Q.; Jin, R.; Luo, Z.; Yang, X.; Liu, Y.; Lu, Q.; Ouyang, Y.; Guo, H. Chlorogenic acid inhibits epithelial-mesenchymal transition and invasion of breast cancer by down-regulating LRP6. *J. Pharmacol. Exp. Ther.* **2023**, *384*, 254–264. [CrossRef] [PubMed]
70. Zeng, A.; Liang, X.; Zhu, S.; Liu, C.; Wang, S.; Zhang, Q.; Zhao, J.; Song, L. Chlorogenic acid induces apoptosis, inhibits metastasis and improves antitumor immunity in breast cancer via the NF-κB signaling pathway. *Oncol. Rep.* **2021**, *45*, 717–727. [CrossRef] [PubMed]
71. Zhou, Y.; Zheng, J.; Li, Y.; Xu, D.P.; Li, S.; Chen, Y.M.; Li, H.B. Natural polyphenols for prevention and treatment of cancer. *Nutrients* **2016**, *8*, 515. [CrossRef] [PubMed]
72. Chimento, A.; De Luca, A.; D'Amico, M.; De Amicis, F.; Pezzi, V. The involvement of natural polyphenols in molecular mechanisms inducing apoptosis in tumor cells: A promising adjuvant in cancer therapy. *Int. J. Mol. Sci.* **2023**, *24*, 1680. [CrossRef] [PubMed]

Disclaimer/Publisher's Note: The statements, opinions and data contained in all publications are solely those of the individual author(s) and contributor(s) and not of MDPI and/or the editor(s). MDPI and/or the editor(s) disclaim responsibility for any injury to people or property resulting from any ideas, methods, instructions or products referred to in the content.